Estimation of Effective Atomic Number using Dual-Energy Imaging of CT Simulator for Radiation Therapy

Bitbyeol Kim [c], Seongmoon Jung[a,b], Jaeman Son[a], Chang Heon Choi [a,b,c], Jung-in Kim [a,b,c], Jong Min Park [a,b,c*]

[a]Department of Radiation Ongology, Seoul National University Hospital, Seoul, Republic of Korea
[b]Biomedical Research Institute, Seoul National University Hospital, Seoul, Republic of Korea
[c]Institution of Radiation Medicine, Seoul National University Medical Research Center, Seoul, Republic of Korea
[*]Corresponding author: leodavinci@naver.com

1. Introduction

For carbon ion therapy, precise estimation of mass density and effective atomic number (EAN) is essential to dose calculation. In the conventional radiotherapy treatment planning system, the most common method to convert computed tomography (CT) values in Houndsfield units (HU) into mass density or electron density is the generation of a single-energy CT (SECT) calibration curve. However, SECT system is unable to differentiate between a change in mass density and a change in chemical composition of tissue [1]. Therefore, this conversion process causes inaccurate dose calculation. On the other hand, applications of dual-energy CT (DECT) offer the possibility to derive the mass density and EAN on a pixel-by-pixel basis [2, 3] that improves the accuracy. Recently, there have been a number of proton therapy dose calculation approaches based on DECT [4-6].

In this study, we aimed to estimate EAN based on DECT with methods of Rutherford el al. [7], Schneider et al. [1], and Joshi et al. [8] and evaluate the accuracy of the estimated EAN.

2. Methods and Results

2.1 EAN Estimation Model

The linear attenuation coefficient which is related to CT number is a function of the material composition, the photon energies, and the mass density. The linear attenuation coefficient of each voxel at a single average energy in diagnosis range can be expressed as:

$$\mu(E) = \rho \cdot \left(C_1 \cdot \frac{Z^n}{E^3} + C_2 \cdot Z \cdot f_{KN}(E) \right)$$

where ρ is the mass density and Z is the atomic number of the single element material in a voxel, C_i is the constant, $n \approx 4$, and $f_{KN}(E)$ is the Klein-Nishina function. The CT number defined as:

$$\text{HU} = 1000 \cdot \left(\frac{\mu}{\mu_w} - 1 \right)$$

where μ_w is the linear coefficient of the water.
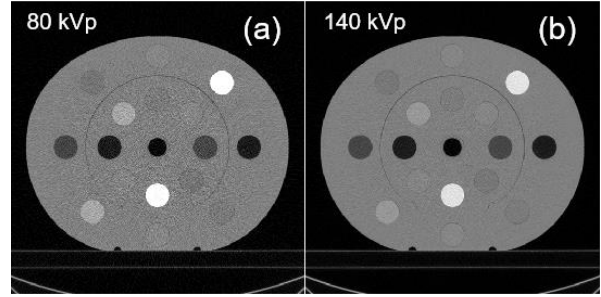
Fig 1. CT images of the CIRS phantom acquired at (a) 80 kVp and (b) 140 kVp tube potentials.

The first method [4, 7] calculated EAN by the following:

$$\frac{\text{HU}_L + 1000}{\text{HU}_H + 1000} = \frac{1 + A Z_{eff}^{m-1}}{B + C Z_{eff}^{m-1}}$$

where HU_L and HU_H are CT numbers at the low and high energy, Z_{eff} is the EAN, A, B, C, and m are fitting parameters.

The second method [1, 5] calculated EAN as below:

$$\frac{\text{HU}_L + 1000}{\text{HU}_H + 1000} = \frac{1 + Z_{eff}^{1.86} \cdot k_{1,L} + Z_{eff}^{3.62} \cdot k_{2,L}}{1 + Z_w^{1.86} \cdot k_{1,L} + Z_w^{3.62} \cdot k_{2,L}}$$
$$\times \frac{1 + Z_{eff}^{1.86} \cdot k_{1,H} + Z_{eff}^{3.62} \cdot k_{2,H}}{1 + Z_w^{1.86} \cdot k_{1,H} + Z_w^{3.62} \cdot k_{2,H}}$$

where Z_{eff} is the EAN of the water and $k_{i,L}$ and $k_{i,H}$ are fitting parameters.

The third method [6, 8] estimated EAN using the ratio between two monoenergetic attenuation coefficients. Because it is independent of the mass density.

2.2 Image acquisition

The electron density phantom (Model 062M, CIRS, Norfolk, VA) was scanned at 80 kVp and 140 kVp tube potentials. The CT simulator (Brilliance CT Big Bore, Philips Medical Systems, Cleveland, OH) was used for scanning. CT images are shown in Fig 1. Phantom dimensions and plug arrangements are shown in Fig 2.
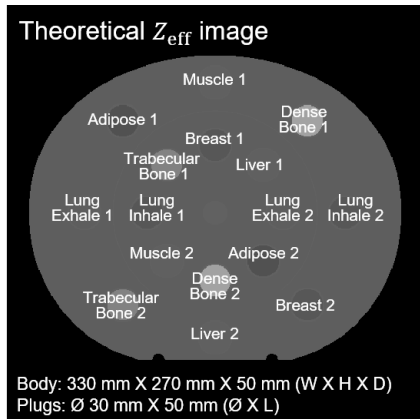
Fig 2. A theoretical EAN image of virtual CIRS phantom.
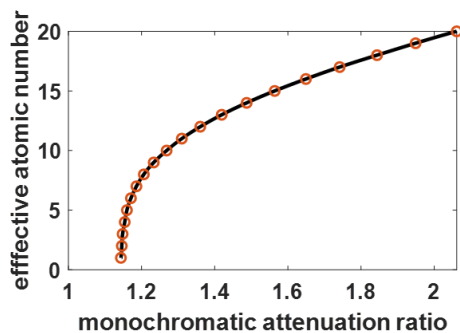
Fig 3. Plot of effective atomic number as a function of the ratio of attenuation coefficients at 80 and 140 keV.

2.3 Calculation

A set of CT images is bilateral filtered for edge-preserving noise reduction and equations are solved for each voxel. Calculations are conducted with CT images before and after noise reduction, respectively. Using the known theoretical EAN, unknown parameters in first and second methods can be obtained. The theoretical EANs of phantom materials are calculated using the mass composition. The theoretical EAN image of a virtual CIRS phantom which has same dimensions and plug arrangements with CT images is shown in Fig 2. The MATLAB optimization toolbox was used to fitting parameters.

For the third method, image-based material decomposition was conducted. 80 keV and 140 keV virtual monoenergetic images are synthesized and used for EAN estimation. The monoenergetic attenuation coefficient ratio of elements was calculated with NIST data [9] and then atomic numbers in typical body range vs monoenergetic attenuation ratios were fitted by polynomial function as shown in Fig 3.

2.4 Evaluation

Estimated EANs of phantom materials were measured using region of interests covering 80 % of the uniform plugs. The relative differences between estimated values without noise reduction and their theoretical values are varied from -2.7% to 85.2%. Results from CT images with noise reduction shows significant improvement. Calculated EAN images with noise reduced CT images are shown in Fig 4. The mean, standard deviation, and relative difference of images are listed in Table I. The relative differences ranged from -4.7% to 5.7% for soft tissue and bone inserts and up to -11.3% for lung inserts. Largest errors are seen with the material simulating lung for both results of CT image sets. The low density of the lung-mimicking inserts is expected to result large spreads.

3. Conclusions

We evaluated the accuracy of EAN estimation with CT simulator using phantom measurements. The noise may result in larger relative differences than one would obtain with a dedicated DECT scanner. Therefore, it is necessary to conduct appropriate noise reduction. Further works such as optimization of tube potential energy pair to acquire a set of CT images are required for more precise estimation.

ACKNOWLEDGEMENT

REFERENCES

[1] W. Schneider, T. Bortfeld and W, Schlegel, "Correlation between CT numbers and tissue parameters needed for Monte Carlo simulations of clinical dose distributions," Physics in Medicine and Biology, 45, 459-478, 2000.
[2] R. E. Alvarez and A. Macovski, "Energy-selective reconstructions in X-ray computerized tomography," Physics in Medicine and Biology, 21(5), 733-744, 1976.
[3] T. R. C. Johnson, "Dual-Energy CT: General Principles," American Journal of Roentgenology, 199(5), S3-S8, 2012.
[4] G. Landry, J. Seco, M. Gaudreault and F. Verhaegen, "Deriving effective atomic numbers from DECT based on a parameterization of the ratio of high and low linear attenuation coefficients," Physics in Medicine and Biology, 58, 6851-6866, 2013.
[5] J. Zhu and S. N. Penfold, "Dosimetric comparison of stopping power calibration with dual-energy CT and single-energy CT in proton therapy treatment planning," Medcal Physics, 43(6), 2845-2854, 2016.
[6] C. Hua, N. Shapira, T. E. Merchant, P. Klahr and Y. Yagil, "Accuracy of electron density, effective atomic number, and iodine concentration determination with a dual-layer dual-energy computed tomography system," Medical Physics, 45(6), 2486-2497, 2018.
[7] R. A. Rutherford, B. R. Pullan and I. Isherwood, "Measurement of effective atomic number and electron density using an EMI scanner," Neuroradiology, 11, 15-21, 1976.
[8] M. Joshi, D. A. Langan, D. S. Sahani, A. Kambadagone, S. Aluri, K. Procknow, X. Wu, R. Bhotika, D. Okerlund, N. Kulkarni, D. Xu, "Effective Atomic Number Accuracy for Kidney Stone Characterization using Spectral CT," Proc.

SPIE, 7622, Medical Imaging 2010: Physics of Medical Imaging, 76223K.

[9] National Institute of Standards and Technology (NIST). XCOM: Photon cross sections database. https:// physics.nist.gov/PhysRefData/Xcom/html/xcom1.html. Accessed January 16, 2020.
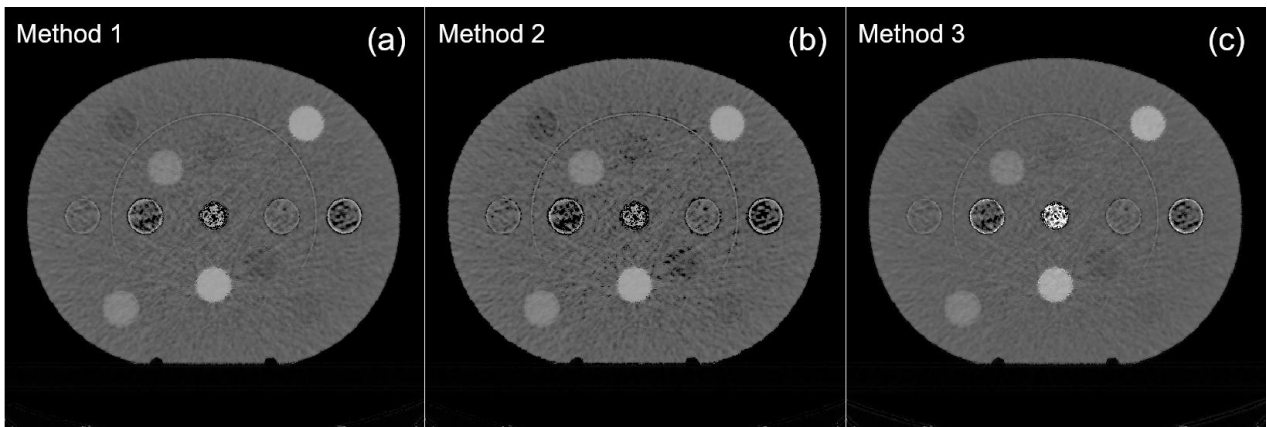
Fig 4. Calculated EAN images with methods of (a) Rutherford el al., (b) Schneider et al., and (c) Joshi et al.

Table I: Results for EANs and their relative differences between estimated values and their theoretical values.

	Theoretical Z_{eff}	Calculated Z_{eff}, Δ (%)					
		Method 1		Method 2		Method 3	
Adipose 1	6.38	6.60 ± 0.52	3.4	6.12 ± 0.92	-4.0	6.75 ± 0.41	5.7
Adipose 2		6.57 ± 0.75	2.9	6.16 ± 1.13	-3.5	6.73 ± 0.59	5.4
Breast 1	6.83	6.82 ± 0.65	-0.1	6.51 ± 0.93	-4.7	6.93 ± 0.51	1.5
Breast 2		7.07 ± 0.42	3.5	6.86 ± 0.59	0.5	7.12 ± 0.34	4.3
Lung Inhale 1	6.83	6.28 ± 1.98	-8.1	6.85 ± 1.89	0.3	6.38 ± 1.78	-6.5
Lung Inhale 2		6.06 ± 1.93	-11.3	6.74 ± 1.62	-1.4	6.16 ± 1.76	-9.8
Lung Exhale 1	7.41	7.38 ± 0.84	-0.4	7.20 ± 1.12	-2.8	7.38 ± 0.68	-0.4
Lung Exhale 2		7.45 ± 1.05	0.5	7.33 ± 1.28	-1.0	7.43 ± 0.90	0.3
Liver 1	7.50	7.54 ± 0.52	0.5	7.44 ± 0.68	-0.8	7.50 ± 0.43	0.0
Liver 2		7.64 ± 0.41	1.8	7.58 ± 0.51	1.1	7.58 ± 0.34	1.1
Muscle 1	7.51	7.59 ± 0.32	1.0	7.53 ± 0.39	0.3	7.54 ± 0.26	0.4
Muscle 2		7.55 ± 0.66	0.6	7.45 ± 0.85	-0.8	7.52 ± 0.53	0.1
Trabecular bone 1	10.18	10.04 ± 0.38	-1.4	10.07 ± 0.37	-1.1	9.70 ± 0.38	-4.7
Trabecular bone 2		10.19 ± 0.29	0.1	10.22 ± 0.28	0.4	9.85 ± 0.30	-3.2
Dense bone 1	12.67	12.66 ± 0.14	-0.1	12.63 ± 0.14	-0.3	13.17 ± 0.25	4.0
Dense bone 2		12.73 ± 0.21	0.5	12.70 ± 0.21	0.3	13.31 ± 0.39	5.0